ELSEVIER

International Journal of Mass Spectrometry 190/191 (1999) 129–143

International Journal of Mass Spectrometry

A new ion ejection method employing an asymmetric trapping field to improve the mass scanning performance of an electrodynamic ion trap

Maurizio Splendore*, Ed Marquette, Jim Oppenheimer, Chuck Huston, Greg Wells

Varian Chromatography Systems, Walnut Creek, CA 94598, USA

Received 28 September 1998; accepted 24 November 1998

Abstract

A new method to eject ions from an electrodynamic ion trap is discussed. An asymmetric trapping field is electronically generated with electrodes, comprised of a ring electrode and two end-cap electrodes having symmetrical hyperbolic surfaces. The asymmetric trapping field is generated by adding an alternating voltage out of phase to each end cap at the same frequency as the ring electrode. The resulting multipole field has a dipole component in the axial direction, as well as a significant hexapole component. All ions confined in the combined trapping field are uniformly displaced away from the geometrical center of the ion trap, defined to be the midpoint along the axis of symmetry between the end-cap electrodes. The displacement is independent of the mass-to-charge ratio of the ions. During mass analysis ions are ejected predominantly through one end-cap electrode and the detected ion signal intensity is doubled. Mass analysis is performed by the application of phase-locked supplementary dipole and quadrupole excitation fields at an operating point corresponding to $\beta_z = 2/3$. Ions at this operating point are simultaneously in resonance with three fields: (1) the nonlinear hexapole trapping field resonance, (2) the parametric resonance with the supplementary quadrupole field, and (3) the sideband resonance with the supplementary dipole field. The simultaneous triple resonance causes extremely fast power absorption by the ions and improved mass resolution. (Int J Mass Spectrom 190/191 (1999) 129–143) © 1999 Elsevier Science B.V.

Keywords: Quadrupole ion trap; Asymmetric trapping field; Multipole trapping field; Nonlinear resonance; Mass scanning

1. Introduction

Ions are confined within an electrodynamic quadrupole field when their trajectories are bounded in the radial (r) and axial (z) directions. The ion motion in the trapping field is nearly periodic. In a pure quadrupole trapping field the ion motions in both the radial and axial directions are independent of each other. The equations of motion for a single ion in the trapping field can be resolved into a pure axial motion and a pure radial motion that have identical mathematical forms described by the Mathieu equation [1]. The Mathieu equation for the axial motion depends on two parameters, a_z and q_z, that characterize the solutions in the axial direction. Similar parameters, a_r and q_r, exist for the radial motions. These parameters define a two dimensional region in (a_i, q_i) space for the coordinate (i), in which the ion motions are bounded and, therefore, stable. For small values of q_i,

* Corresponding author. E-mail: maurizio.splendore@csb.varian.com

Dedicated to J.F.J. Todd and R.E. March in recognition of their original contributions to quadrupole ion trap mass spectrometry.

PII S1387-3806(99)14291-4

the pseudoharmonic motion of an ion can be characterized by the dominant fundamental frequency [1] of ion motion in the (i) coordinate. A point in (a_i, q_i) space defines the operating point for the ion. The amplitude of the ion motion in the radial or axial direction can be increased by the application of a supplementary alternating field having a frequency and symmetry that is in resonance with one of the frequencies of the ion motion. If the amplitude of the ion motion is increased enough, the ion will be driven to the surface of an electrode. If a hole exists in the electrode where the ion is directed, it can escape the trapping field altogether and exit the trap.

March et al. [2,3] used *dipolar resonant excitation* to eject unwanted ions from a quadrupole ion trap. In these studies, a supplementary alternating voltage was applied to the end-cap electrodes of the ion trap, out of phase, to produce an alternating dipole field in the axial direction. Resonant ejection occurs only for those ions having an axial frequency of motion equal to the frequency of the supplementary alternating field. The ions in resonance with the supplementary field increase the amplitude of their axial oscillation until the kinetic energy of the ions exceed the restoring force of the rf trapping field and ion ejection occurs in the axial direction.

Jefferts [4] used a quadrupole ion trap to distinguish ions of different mass-to-charge ratios that were formed by photodissociation inside the trap. The trapping field frequency was swept and ions of successive mass-to-charge ratios were made unstable in the axial direction. Ions were sequentially ejected from the ion trap and detected by an electron multiplier. Subsequently, Ensberg and Jefferts [5] used dipolar resonant excitation to eject ions from the trap to an external detector by applying an axial resonant field to the end-cap electrodes. The frequency of the applied field was swept and ions of successive mass-to-charge ratios were ejected from the trap. A variant of these methods is used in commercial ion trap mass spectrometers to eject ions by dipolar resonant excitation [6,7]. The amplitude of the rf trapping field is increased linearly to increase the operating point (q_z, a_z) of the ions until the fundamental frequency of ion motion comes into resonance with a supplementary alternating voltage on the end-cap electrodes and resonant ejection occurs.

Ion ejection by *quadrupolar resonant excitation* can be effected by the application of a supplementary alternating voltage applied in phase to the end-cap electrodes. *Parametric resonant excitation* by a supplementary quadrupole field causes ion amplitudes to increase in the axial direction when the ion frequency is one half of the supplementary quadrupole frequency [8]. Parametric resonant excitation has been investigated theoretically [8,9]. The supplementary quadrupole field has a value of zero at the center of the ion trap. When a buffer gas such as helium is used to dampen the ion trajectories to the center of the trap, parametric excitation is ineffectual because of the vanishing strength of the supplementary quadrupole field. In order to have a finite excitation force applied to the ions, it is necessary to displace them from the center of the supplementary quadrupole field to a location where the field has a nonzero value.

A weak resonant dipole field having a frequency of one half of the parametric frequency displaces ions from the center of the trap when the operating point of the ions is changed to bring the ion fundamental frequency into resonance with the dipole field [10]. Since the parametric frequency is twice the dipole frequency the ion will absorb power from the supplementary quadrupole field. This mode of ion ejection, in which power is absorbed sequentially from the dipole and then the quadrupole field, is adequate for ion ejection in a constant trapping field, where the fundamental frequency of the ion motion is not changing because of the amplitude of the rf field. However, it is not optimal when the trapping field amplitude is changing, as is normally the case for mass scanning. In this case, the rf trapping field amplitude is increased to raise the fundamental frequency of the ion motion, bringing it into resonance first with the dipole field. The dipole field displaces the ion from the center of the trap, where the quadrupole field is zero. After the ion has been displaced from the center, it can then absorb power from the supplementary quadrupole field if it is in resonance with the parametric resonance. Therefore, it is necessary to fix the dipole resonant frequency at a value

less than one half of the parametric resonance [11] so that, as the fundamental frequency of the ion motion is increased, by increasing the trapping field rf amplitude, the ion motion will sequentially be in resonance with the dipole field, and then with the quadrupole field.

The geometry of the commercial ion trap electrodes has been modified to introduce an octapole component into the trapping field to enhance mass resolution [12]. Higher-order fields can be obtained by increasing the separation between the end-cap electrodes while maintaining ideal hyperbolic surfaces [13]. These surfaces have asymptotes at 35.26° with respect to the symmetric radial plane of the ion trap. Alternatively, the surfaces of the end-cap electrodes can be shaped with an angle of 35.96° [14–16] while maintaining the ideal separation between the end-cap electrodes. For either geometry the trapping field is symmetric with respect to radial plane.

In this work a new ion ejection method [17] that uses a trapping field asymmetric with respect to the radial plane is presented [18,19]. The asymmetric trapping field is generated by adding an alternating voltage out of phase to each end-cap electrode at the same frequency as the ring electrode. This trapping field dipole component (TFD) causes the center of the trapping field to not coincide with the geometric center of the ion trap electrode assembly. The first order effect of adding the dipole component to the trapping field is to displace the ions toward the end-cap electrode that has the TFD component in phase with the rf voltage applied to the ring electrode. A second order effect is to superimpose a substantial hexapole field [20,21]. The resulting multipole trapping field has a nonlinear resonance at the operating point of $\beta_z = 2/3$ [16,22,23]. Since the ions are already displaced from the geometrical center of the trap by the asymmetric trapping field, the hexapole resonance has a finite value where the ions reside. Likewise, at this operating point, a parametric resonance attributed to a supplementary quadrupole field will also have a nonzero value. Finally, the addition of a supplementary dipole field at this point will also cause dipolar resonant excitation. All three fields will have nonzero values at the operating point of $\beta_z = 2/3$ and, therefore, a triple resonance condition exists. An ion moved to this operating point will be in resonance with, and absorb power from, all three fields simultaneously.

At the operating point of the triple resonance, power absorption by the ions is nonlinear. The amplitude of the axial ion motion also increases nonlinearly and the ion is quickly ejected from the trap. Ion trajectories are less effected by collisions with the damping gas in the region of the resonance, and resolution is improved. The displacement of the trapping center towards the exit end cap causes the ions to be ejected exclusively through this electrode, thus doubling the number of ions detected.

2. Experimental

All experiments were performed using commercial Varian QISMS and Varian Saturn 2000 Ion Traps (Varian Chromatography Systems, Walnut Creek, CA) modified with appropriate prototype hardware [17,18]. The TFD with the appropriate drive frequency was generated by a voltage divider network. The voltage divider used the rf voltage applied to the ring electrode to supply an out-of-phase voltage on each end-cap electrode. The voltage divider was comprised of the capacitance between the ring electrode and each end-cap electrode, and an impedance from each end-cap electrode to ground. The impedance to ground on the multiplier end-cap electrode was capacitive, whereas the impedance to ground on the filament end-cap electrode was inductive. The TFD could be turned off by shunting the impedance to ground. The nonlinear hexapole resonance at $\beta_z = 2/3$ could be turned on and off by controlling the TFD.

A supplementary alternating quadrupole field was applied in phase to the end-cap electrodes with a frequency that was 2/3 of the drive frequency and provided the parametric resonance. A supplementary alternating dipole field was applied out of phase to the end-cap electrodes with a frequency that was 2/3 of the drive frequency and provided the sideband resonance. The TFD and the supplementary fields were

phase-locked to the drive frequency of the trapping field.

SATURN REVISION C software was used to control the QISMS ion trap whereas the Saturn 2000 Workstation (Varian Chromatography Systems, Walnut Creek, CA), modified to control the TFD, was used to control the Saturn 2000 Ion Trap. Ion signal intensity and mass peak shape data were obtained from a Tektronik model DSA 602A digitizing signal analyzer.

The samples used were perfluro-tri-n-butylamine (FC-43), hexachlorobenzene (HCB), and undecane. HCB and undecane were introduced via the Varian Chromato-Probe and temperature was controlled by a Varian 3400 GC. Generally, the ion trap was operated at a temperature of 150 °C. The approximate pressure in the ion trap was calculated to be 2.0 mTorr based on the ion trap conductance, pumping speed for helium, and the measured column flow rate of 1.0 atm-cm^3/min. Simulations of ion motion were performed using SIMION VERSION 6.0 (D.A. Dahl; Idaho National Engineering Laboratory, Idaho Falls). Fourier transforms of the simulated ion motions were accomplished using MATHCAD 5.0 (MathSoft Inc., Cambridge, MA).

3. Results and discussion

3.1. Electrodynamic trapping field

The canonical form of the electrodynamic trapping potential for a time dependent field in a cylindrical coordinate system (r, z) is given by [24]:

$$V_T(r, z, t) = \sum_{N=0}^{\infty} A_N \Phi_N(r, z)\Pi(t) + \sum_{N=0}^{\infty} B_N U_N(r, z) \quad (1)$$

where $\Pi(t) = \cos(\Omega t)$ expresses the temporal variations of the field with drive frequency Ω; $\Phi_N(r, z)$ and $U_N(r, z)$ represent the dynamic and static spatial variations of the field and A_N, B_N the normalized constants, respectively. The spatial terms are related to the Legendre polynomials $P_N \cos(\theta)$ of order N [24]. In a field with rotational symmetry, the potential is independent of the angle φ. The terms of the polynomial are expressed here as a function of the cylindrical coordinates (r, z) and the arbitrary distance s necessary to fix the boundary conditions [25]:

Dipole $$P_1(\cos\theta) = -z/s \quad (2a)$$

Quadrupole $$P_2(\cos\theta) = (r^2 - 2z^2)/2s^2 \quad (2b)$$

Hexapole $$P_3(\cos\theta) = (3r^2z - 2z^3)/2s^3 \quad (2c)$$

Octapole $$P_4(\cos\theta) = -(3r^4 - 24r^2z^2 + 8z^4)/8s^4 \quad (2d)$$

Deacapole $$P_5(\cos\theta) = -(15r^4z - 40r^2z^3 + 8z^5)/8s^5 \quad (2e)$$

Dodecapole $$P_6(\cos\theta) = (5r^6 - 90r^4z^2 + 120r^2z^4 - 16z^6)/16s^6 \quad (2f)$$

An ideal hyperbolic ion trap with electrodes extending to infinity would only have the quadrupole term Eq. (2b), with $N = 2$ in Eq. 1. Real ion traps with electrodes of finite extent will have additional terms with $N > 2$. Terms with order greater than 2 will cause a coupling between the radial and axial ion motion. The superposition of multipole fields will generate nonlinear resonances in the trapping field. When the operating point of the ion motion is at a nonlinear resonance, ions may absorb energy from the trapping field alone and their motion can increase in amplitude.

Wang [26,27] has shown that nonlinear resonances in the trapping field are found when:

$$n_r\omega_r + n_z\omega_z = \nu\Omega$$

where ω_r and ω_z are the radial and secular frequencies and ν, n_r, and n_z are integers. In particular, the next highest multipole field after the quadrupole is the hexapole, $N = 3$, Eq. (2c). The use of this nonlinear resonance to axially eject ions from the ion trap has been discussed in detail by Franzen [23,28,29], where the hexapole component has been increased by shaping the end-cap electrodes with a different angle.

Referring to Eq. (2), it can be seen that all multipole fields greater than the quadrupole have a zero value at the center of the ion trap.

The general form of the equations of motion can be obtained from the vector equation:

$$m\frac{\partial^2\vec{R}}{\partial t^2} + e\vec{\nabla}V_T = 0 \tag{3}$$

where the position vector is $\vec{R}(r, z)$, m is the ion mass and e is the charge of the ion.

For an ideal quadrupole trapping field extending to infinity $A_N = 0$ and $B_N = 0$ for all N, except $N = 2$ [Eq. (1)] when the periodic voltage $\Pi(t) = \cos(\Omega t)$ and the dc voltage U are applied to the ring electrode and the end-cap electrodes are grounded. The potential inside the ion trap, $V_T(z, r, t) = V_{\mathrm{TFQ}}$, is given from:

$$V_{\mathrm{TFQ}} = \frac{V_{\mathrm{ac}}}{(r_0^2 + 2z_0^2)}[r^2 - 2(z^2 - z_0^2)] \times \cos(\Omega t) + \frac{U}{(r_0^2 + 2z_0^2)}[r^2 - 2(z^2 - z_0^2)] \tag{4}$$

where V_{ac} is the zero-to-peak amplitude of the electrodynamic potential with frequency Ω, r_0 is the radius of the ring electrode, and z_0 is the separation of the end-cap electrodes from the origin. The equations of the ion motion for this case allow the separation of the motion into the radial and axial components. The axial equation of motion for an ion is described by the following differential equation:

$$\frac{\partial^2 z}{\partial t^2} - \left(\frac{e}{m}\right)\left(\frac{4U}{r_0^2 + 2z_0^2}\right)z - \left(\frac{e}{m}\right)\left(\frac{4V_{\mathrm{ac}}}{r_0^2 + 2z_0^2}\right)z[\cos(\Omega t)] = 0 \tag{5}$$

Defining the dimensionless parameters ζ, q_z, and a_z [1] as:

$$\zeta = \frac{\Omega t}{2} \tag{6a}$$

$$q_z = +8eV_{\mathrm{ac}}/[m(r_0^2 + 2z_0^2)\Omega^2] \tag{6b}$$

$$a_z = -16eU/[m(r_0^2 + 2z_0^2)\Omega^2] \tag{7}$$

and substituting the ζ, q_z, and a_z in Eq. (5), the equation of motion for an ion can be rearranged to Eq. (8):

$$\frac{d^2 z}{d\zeta^2} + [a_z - 2q_z\cos(2\zeta)]z = 0 \tag{8}$$

This second order differential equation is the well known Mathieu equation [1]. The stable solutions to the equation in the axial direction are characterized by the parameters q_z and a_z that define the operating point of an ion within the stability region. The general solution to Eq. (4) is:

$$z(\zeta) = A\sum_{n=-\infty}^{+\infty} C_{2n}\cos(2n + \beta_z)\zeta + B\sum_{n=-\infty}^{+\infty} C_{2n}\sin(2n + \beta_z)\zeta \tag{9}$$

The secular frequency of ion motion, $\omega_{z,0}$, can be determined from the value of β_z [4]:

$$\omega_{z,n} = (n \pm \beta_z/2)\Omega \tag{10}$$

The value of β_z is a function of the working point in (a_z, q_z) space and can be computed from a well known continuing fraction [1].

3.2. Dipole component of the trapping field

To simplify the equations, it is assumed that the ion trap is operated without the dc field, so that in Eq. (4), $U = 0$. When the dipole component of the trapping field (TFD), V_{TFD} [Eq. (2a)], is superimposed on the quadrupole trapping field, V_{TFQ} [Eq. (4)], the potential inside the ion trap $V_T(z, r, t)$, in the vicinity of the axial axis, can be expressed as:

$$V_T(z, r, t) = V_{\mathrm{TFQ}} + V_{\mathrm{TFD}} = \frac{V_{\mathrm{ac}}}{(r_0^2 + 2z_0^2)} \times [r^2 - 2(z^2 - z_0^2)]\cos(\Omega t) + \frac{V_{\mathrm{da}}z}{z_0}\cos(\Omega t + \varphi) \tag{11}$$

where V_{da} is the zero-to-peak amplitude of the TFD applied across the end-cap electrodes. The TFD is phase shifted by $+\varphi$ with respect to the quadrupole trapping field, V_{TFQ}. Restricting the phase to values of $\varphi = N\pi$, where $N = 0, 1, 2,—$, $V_d = V_{da}(-1)^N$. The instantaneous electric field acting on an ion in the axial direction because of the trapping field $V_T(z, r, t)$ is:

$$E_z = -\frac{\partial V}{\partial z} = -\left(-\frac{4V_{ac}}{(r_0^2 + 2z_0^2)}z + \frac{V_d}{z_0}\right)\cos(\Omega t) \tag{12}$$

The equation of the ion motion becomes:

$$m\frac{d^2z}{dt^2} = -e\left(-\frac{4V_{ac}}{(r_0^2 + 2z_0^2)}z + \frac{V_d}{z_0}\right)\cos(\Omega t) \tag{13}$$

Substituting $\zeta = \Omega t/2$ in Eq. (13) yields:

$$\frac{d^2z}{dt^2} = \frac{\Omega^2}{4}\frac{d^2z}{d\zeta^2} \tag{14}$$

The basic equation of ion motion in the axial direction is obtained by substitution of Eq. (14) in Eq. (13) and $2\zeta = \Omega t$:

$$\frac{d^2z}{d\zeta^2} = \frac{4e}{m\Omega^2}\left(\frac{4V_{ac}}{(r_0^2 + 2z_0^2)}z - \frac{V_d}{z_0}\right)\cos(2\zeta) \tag{15}$$

Rearranging gives:

$$\frac{d^2z}{d\zeta^2} - \left[2\left(\frac{8eV_{ac}}{m(r_0^2 + 2z_0^2)\Omega^2}z - \frac{2eV_d}{mz_0\Omega^2}\right)\right]\cos(2\zeta) = 0 \tag{16}$$

Defining:

$$q_z = \frac{8eV_{ac}}{m(r_0^2 + 2z_0^2)\Omega^2} \tag{17a}$$

$$q_d = -\frac{2eV_d}{mz_0\Omega^2} \tag{17b}$$

By substitution of Eq. (17a) and Eq. (17b) into Eq. (16), an equation similar to the Mathieu equation is obtained:

$$\frac{d^2z}{d\zeta^2} - 2(q_z z + q_d)\cos(2\zeta) = 0 \tag{18}$$

The following definition and substitutions: $u = (q_z z + q_d)$ and $d^2u/d\zeta^2 = q_z(d^2z/d\zeta^2)$ into Eq. (18) yields this form of the Mathieu equation:

$$\frac{d^2u}{d\zeta^2} - 2q_z\cos(2\zeta)u = 0 \tag{19}$$

The axial displacement of the ion can be found to be the sum of two terms:

$$z = \frac{u - q_d}{q_z} = \frac{u}{q_z} - \frac{q_d}{q_z} \tag{20}$$

where the first term represents the normal time dependent oscillatory solution, $u(\zeta)$ as in Eq. (9). The second term is an additive offset value that expresses the axial displacement of the ion motion because of the TFD:

$$-\frac{q_d}{q_z} = -\left(-\frac{2eV_d}{mz_0\Omega^2}\right)\left[\frac{m(r_0^2 + 2z_0^2)\Omega^2}{8eV_{ac}}\right] = \frac{(r_0^2 + 2z_0^2)V_d}{4z_0V_{ac}} \tag{21}$$

During mass analysis ions are sequentially ejected at the same operating point q_z, thus, V_{ac}/m will be constant. In the special case in which $V_d = \eta V_{ac}$, Eq. (21) becomes:

$$-\frac{q_d}{q_z} = \frac{r_0^2 + 2z_0^2}{4z_0}\eta$$

giving:

$$z = \frac{u}{q_z} + \frac{r_0^2 + 2z_0^2}{4z_0}\eta \tag{22}$$

When the TFD is properly phased and present as a constant fraction η of the trapping field, it can be seen from Eq. (22) that the ion motion is uniformly displaced in the axial direction by a constant amount. The magnitude and sign of the displacement is independent of the mass-to-charge ratio and the charge polarity of the ion. The displacement depends only on the percentage η of TFD and the geometry of the ion

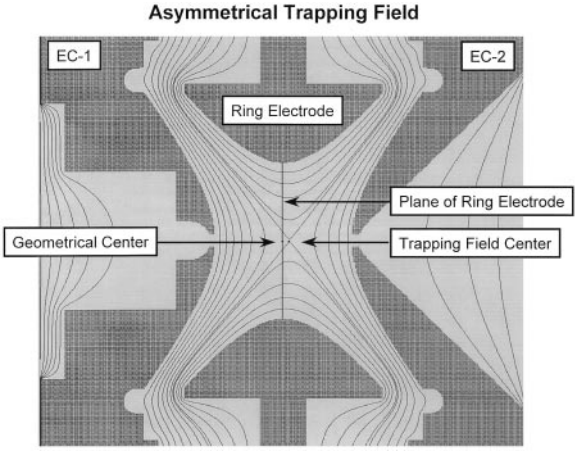

Fig. 1. Equipotential lines in a trapping field with a 15% TFD. EC-1 = −1.15 V; EC-2 = −0.85 V; ring electrode = +1.0 V.

trap assembly. The direction of the displacement can be altered by changing the phase of the dipole from 0 to π.

The first order effect of adding the dipole component to the trapping field is to displace the ions toward the end-cap electrode that has the TFD component in phase with the rf applied to the ring electrode. Fig. 1 shows a SIMION calculation of equipotential surfaces of the Saturn 2000 electrodes, using $r_0 = 10$ mm and $z_0 = 7.07$ mm to define the hyperbolic surfaces. The ring electrode has a potential of 1 V, the end-caps have −1.15 and −0.85 V potentials, and the entire electrode assembly is surrounded by a grounded cylinder (not shown). The potential on the end caps creates a 15% TFD along the z axis. The end-cap electrodes were displaced an additional 0.75 mm along the z axis, away from the center. This is often referred to as the "stretched trap" geometry [13]. The equipotential lines plotted in Fig. 1 show that the trapping field center is displaced towards the multiplier electrode. Additionally, the axial pseudopotential well is lower towards the multiplier end-cap electrode relative to the filament electrode. Therefore, ions will approach the multiplier end-cap electrode closer than the filament electrode. The ions will be ejected preferentially through the exit hole on the multiplier electrode since their kinetic energy first exceeds the axial restoring force of the multiplier electrode. Unidirectional ion ejection with the TFD can be experimentally observed when the ejection occurs by axial instability at $\beta_z = 1$, or when resonance ejection occurs using a supplementary dipole field at lower operating points.

The coefficients of the first six terms of the multipole expansion of the potential field, Eq. (1), were determined from the potential field calculated by SIMION, and a multivariate regression fit of the potentials to Eq. (1). The potentials at the grid points in a selected rectangular region along the z axis were used in the regression fit to the first six terms in Eq. (1). Table 1 lists the coefficients calculated for four different electrode conditions. The coefficients for the asymmetric trapping field, reported in the last column of Table 1, were calculated for a truncated,

Table 1
A_N coefficients

		Trapping field geometry			
N	Multiple field	Ideal[a]	Truncated[b]	Stretched[c]	Asymmetric[d]
0	Monopole	0	0	0.112	0.112
1	Dipole	0	0	0	−0.10
2	Quadrupole	−2	−2.003	−1.71	−1.75
3	Hexapole	0	0	0	−0.04
4	Octapole	0	0.004	−0.035	−0.03
5	Decapole	0	0	0	−0.008

[a] Ideal ion trap geometry with hyperbolic electrode surfaces extended to infinity, $r_0^2 = 2z_0^2$ with $r_0 = 10$ mm.
[b] Ion trap geometry with hyperbolic electrode surfaces truncated such that the length of the asymptotes is $2.8r_0$, with $r_0 = 10$ mm.
[c] Ion trap geometry like b) with $2z_0 = 15.64$ mm.
[d] Ion trap geometry like c) with a 15% TFD.

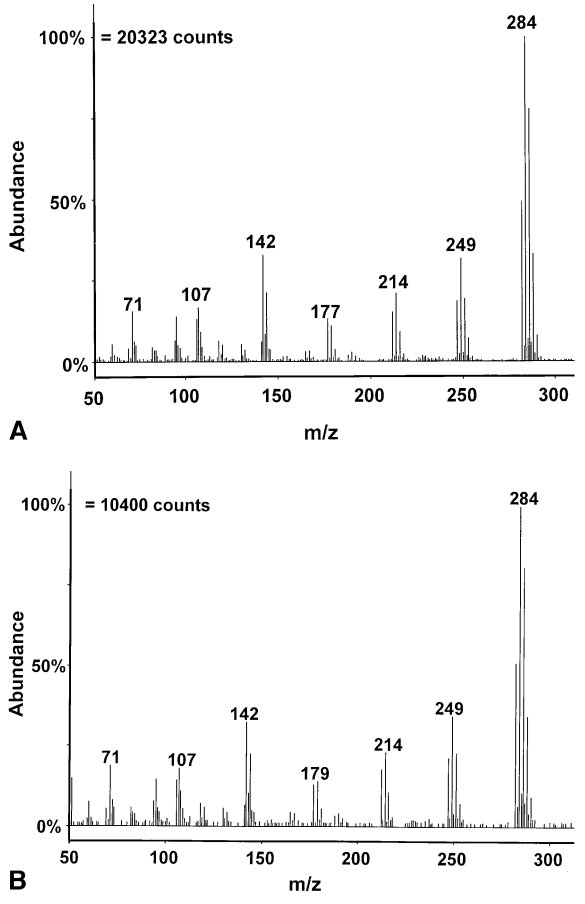

Fig. 2. Mass spectra of hexachlorbenzene obtained with a supplementary dipole amplitude of 4 $V_{(p-p)}$ and frequency of 485 kHz. (a) TFD = 15%; base peak is 20 323 ion counts. (b) The TFD = 0; base peak is 10 400 ion counts.

"stretched" geometry with a 15% TFD. It can be seen that the truncation of the hyperbolic surfaces introduced even-order multipole fields, predominately a positive octapole field. The "stretched" geometry had an octapole component that changes sign. Moreover, for the stretched and asymmetric trapping field geometry, a positive monopole term was obtained. In addition to the large dipole coefficient obtained when the TFD is present, a substantial negative hexapole coefficient of -0.04 was found.

The mass spectra of HCB, shown in Fig. 2, were obtained by applying a supplementary dipole field between the end-cap electrodes that had a frequency of 485 kHz. The mass spectra in Fig. 2(a) and (b) were obtained with and without a 15% TFD, respectively. In both mass spectra, the characteristic chlorine isotopic cluster was observed because of the molecular ion: $C_6Cl_6^{\cdot+}$ with *m/z* 282, 284, 286, 288, and 290; the fragment ions: $C_6Cl_5^+$ with *m/z* 247, 249, 251, and 253; $C_6Cl_4^{\cdot+}$ with *m/z* 212, 214, and 216; $C_6Cl_3^+$ with *m/z* 177, 179, and 181; $C_6Cl_2^{\cdot+}$ with *m/z* 142 and 144; and C_6Cl^+ with *m/z* 107 and 109. The relative ion abundance was identical in both mass spectra. However, the absolute abundance of all ions was doubled when the TFD was added. Unidirectional ejection was also observed with the TFD, in the absence of the supplementary dipole field, when ions were ejected at the stability boundary at $\beta_z = 1$.

The axial trajectory of an ion of *m/z* = 100 confined in a stretched ion trap with an asymmetric trapping field was computed using SIMION. The TFD was 15%, the trap frequency was 1050 kHz, and the operating point of the ion in the stability diagram was $\beta_z = 0.51$. The axial excursion of the ion was 6 mm from the center of the field. The frequency spectrum of the ion trajectory shown in Fig. 3 was obtained by Fourier analysis of 4k data points of the ion trajectory. The frequency spectrum ranged from 0–2000 kHz, and the fundamental secular frequency of the ion motion $\omega_{z,0}$, was observed at approximately 270 kHz. The two sidebands, $\Omega - \omega_{z,0}$ and $\Omega + \omega_{z,0}$, were observed as expected. Because the TFD introduced a hexapole component in the trapping field, the drive frequency Ω, at 1050 kHz, and the second, third, and fourth harmonics, $2\omega_{z,0}$, $3\omega_{z,0}$, and $4\omega_{z,0}$, were also observed. This was expected from the superposition of odd-multipole components on the trapping field [23,28–30]. The sidebands $\Omega - 3\omega_{z,0}$, $\Omega - 2\omega_{z,0}$, $\Omega + 2\omega_{z,0}$, were also observed with lower intensity. The more intense sidebands of higher harmonics, $2\Omega - \omega_{z,0}$, $2\Omega - 2\omega_{z,0}$, $2\Omega - 3\omega_{z,0}$, $2\Omega - 4\omega_{z,0}$, were also observed. Franzen [12] reported a remarkably similar frequency spectrum obtained from a modified angle ion trap with nonideal electrodes.

A greater influence from the odd-order fields was expected when increasing the percentage of the TFD. The advantage of forming the TFD electronically was that the circuit could be adjusted so that the percentage of TFD added could be varied. Fig. 4 shows the

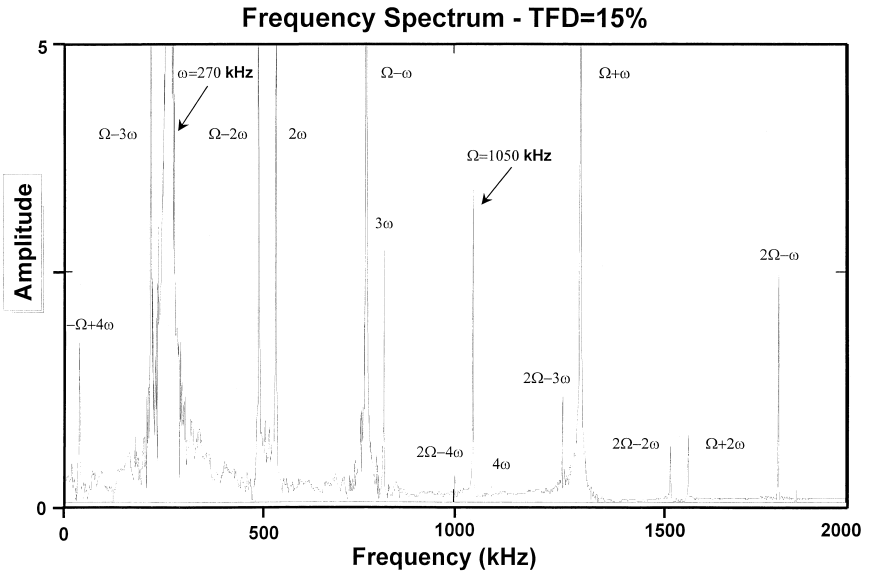

Fig. 3. Frequency spectrum obtained by Fourier analysis of the calculated ion trajectory in a trapping field with 15% TFD. The operating point is $\beta_z = 0.51$ for an ion having *m/z* 100, and a trapping frequency of 1050 kHz. The fundamental secular frequency $\omega_{z,0}$ is 270 kHz.

experimental mass spectrum of CF_3^+ (*m/z* 69 from FC-43) and the effect of varying the TFD from 0–49%, with no supplementary voltages applied to the end-caps. The helium damping gas pressure was maintained at 2 mTorr. In Fig. 4(a) there was no TFD and the ions were ejected only at the stability boundary, $\beta_z = 1$. Figs. 4(b)–4(d) show that the effect of increasing the TFD component was to eject more of the ions at the nonlinear resonance at $\beta_z = 2/3$. The damping gas "cooled" the ions to the center of the trapping field. However, since the center of the trapping field was displaced from the geometrical center of the trap electrodes, the hexapole nonlinear resonance had a nonzero strength and many of the ions are ejected at $\beta_z = 2/3$.

Fig. 5(a) shows the effect of different percentages of TFD on the signal intensity of *m/z* 69 (FC-43) as a function of the amplitude of the supplementary dipole field at a frequency of 700 kHz ($\Omega - \omega_{z,0}$). Ion ejection at $\beta_z = 2/3$ was the result of the double resonance of the sideband resonance from the supplementary dipole field, and the hexapole nonlinear resonance of the trapping field. The phase relationship between the supplementary dipole and trapping field was optimized to maximize signal intensity. In the absence of any TFD, the threshold voltage required to eject ions at $\beta_z = 2/3$ was 5 $V_{(p-p)}$. Acceptable resolution was obtained when the amplitude was 15 $V_{(p-p)}$. As the TFD content in the trapping field was increased, the threshold for ion ejection was observed to decrease. The reduction of threshold voltage was a consequence of the increased strength of the hexapole nonlinear resonance, as well as the increased displacement of the ions from the geometrical center. Similar results were obtained with *m/z* 414 (FC-43). Fig. 5(b) shows similar results for quadrupolar resonant excitation.

Fig. 6(a) shows the spectrum of FC-43 with 15% TFD and with a 2 $V_{(p-p)}$ dipolar resonant excitation at a frequency of 700 kHz ($\Omega - \omega_{z,0}$). Because the amplitude of the supplementary voltage was near the ejection threshold [see Fig. 5(a)] most of the ions were ejected at the stability boundary, at $\beta_z = 1$, rather than at the $\beta_z = 2/3$ nonlinear resonance. The mass spectrum obtained without the dipolar resonant excitation was similar to the one shown in Fig. 6(a). Fig. 6(b) shows the mass spectrum using double resonance with a supplementary quadrupole field having an amplitude of 10 $V_{(p-p)}$ and frequency of 700 kHz ($2\omega_{z,0}$). This voltage was far above the

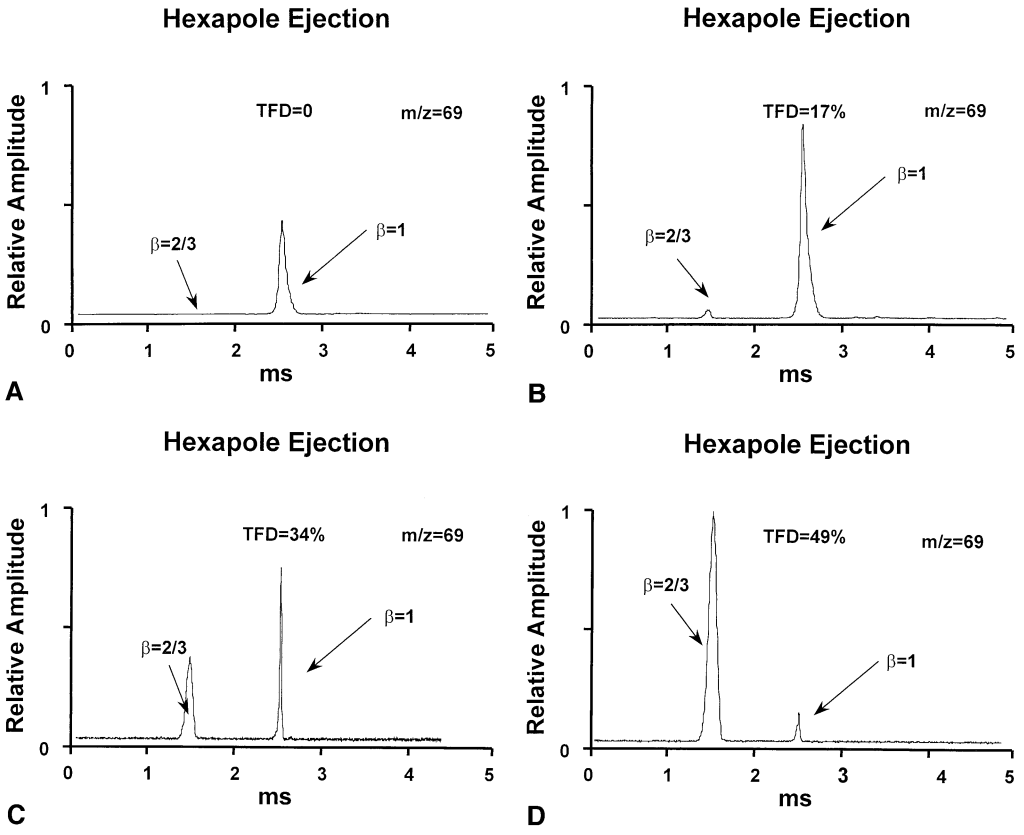

Fig. 4. Mass spectrum of *m/z* 69 of FC-43 with no supplementary field. (a) TFD = 0%; (b) TFD = 17%; (c) TFD = 34%; (d) TFD = 49%.

ejection threshold [see Fig. 5(b)]. The parametric resonance and the hexapole trapping field resonance produced good resolution because the ions had been displaced from the center of the trap and were simultaneously in resonance. The mass spectrum in Fig. 6(c) resulted from combining the supplementary dipole and quadrupole excitation fields used in Fig. 6(a) and (b) to effect a triple resonance.

Table 2 summarizes the operating conditions for the dipolar resonant ejection and triple resonant ejection modes. The dipolar resonant ejection mode operating point was at $\beta_z = 0.92$, and the trapping frequency was 1050 kHz. The fundamental secular frequency, $\omega_{z,0} = 485$ kHz, was very close to the first sideband frequency, $\Omega - \omega_{z,0} = 565$ kHz. The contribution to the ion motion in the axial direction for both these frequencies C_{2n}, Eq. (9), is almost identical since these coefficients approach 1 when β_z is increased to 0.92. The amplitudes of both axial motions were quite large and the resulting beat frequency, $\Delta\omega = \Omega - 2\omega_{z,0} = 80$ kHz could be observed in the ion signal profile. The triple resonance ejection used an operating point at $\beta_z = 2/3$, and the first sideband frequency was 700 kHz, which is far apart from the fundamental frequency of ion motion, 350 kHz. As a consequence, the beat frequency at 350 kHz was easily removed from the detected ion signal by electronic filtering.

Two simulations of the ion trajectory for *m/z* 100 were computed to compare the dipolar resonant ejection and the triple resonant ejection modes using the conditions of Table 2. The model included collisions with the helium buffer gas having a Boltzmann velocity distribution and a Langevin cross section, with isotropic scattering in the center of mass that was transformed into the laboratory coordinates. All fields

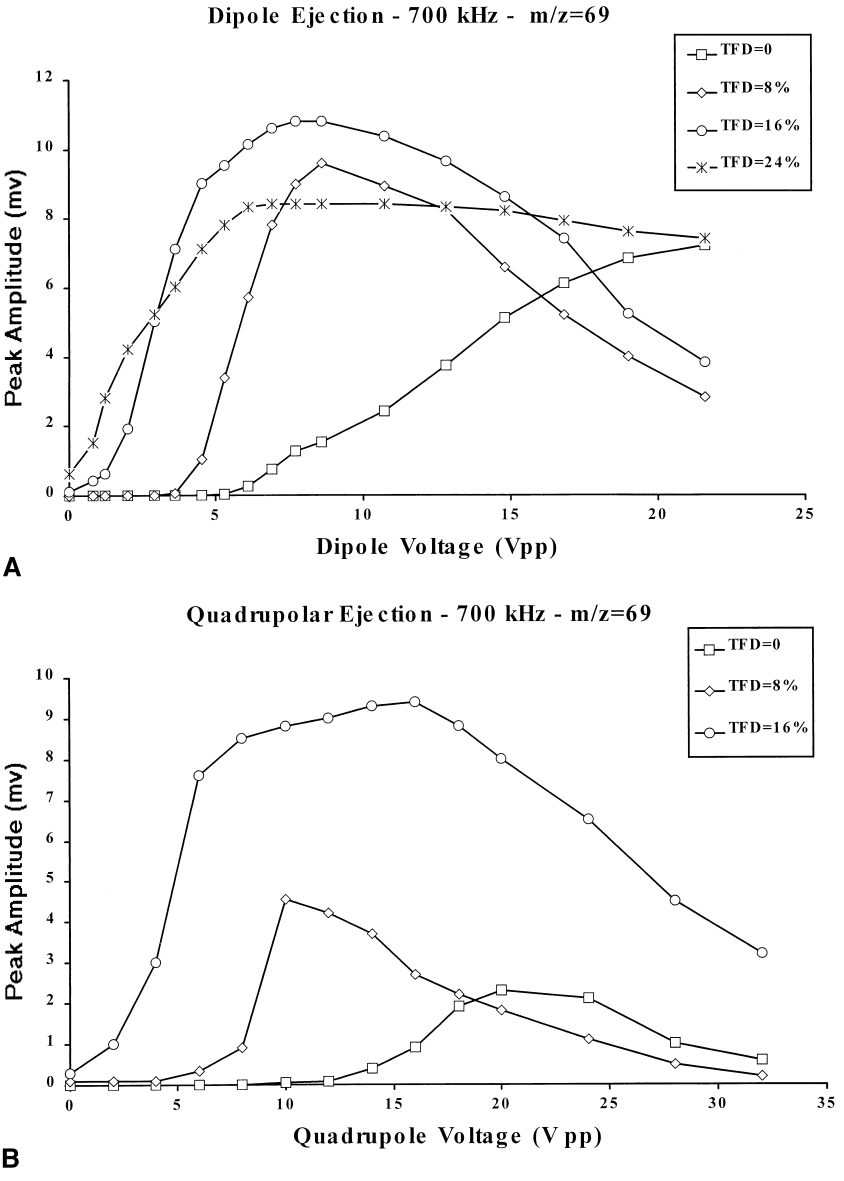

Fig. 5. Ion signal intensity of *m/z* 69 (FC-43) ejected at $\beta_z = 2/3$ as a function of the amplitude of the 700 kHz supplementary field applied to the end-cap electrodes. Each curve is obtained with a different percentage of TFD. Ion are ejected by a double resonance with the hexapole resonance of the trapping field: (a) the dipolar sideband resonance $\Omega - \omega_{z,0}$; (b) the parametric resonance $2\omega_{z,0}$ because of the supplementary quadrupole field.

were generated using the stretched geometry for both ion ejection modes. Initially, the operating point was $\beta_z = 0.25$ and the ion underwent approximately 70 collisions with the helium atoms during a 1 ms cooling period. The rf trapping voltage was increased in 0.1 ms to an operating point corresponding to 7 Da below either $\beta_z = 2/3$ or $\beta_z = 0.92$. Thereafter, the rf trapping voltage was increased with a rate of 0.18 ms/Da.

The ion trajectory was calculated in three dimensions and the axial displacement and kinetic energy for dipolar resonant excitation without TFD are

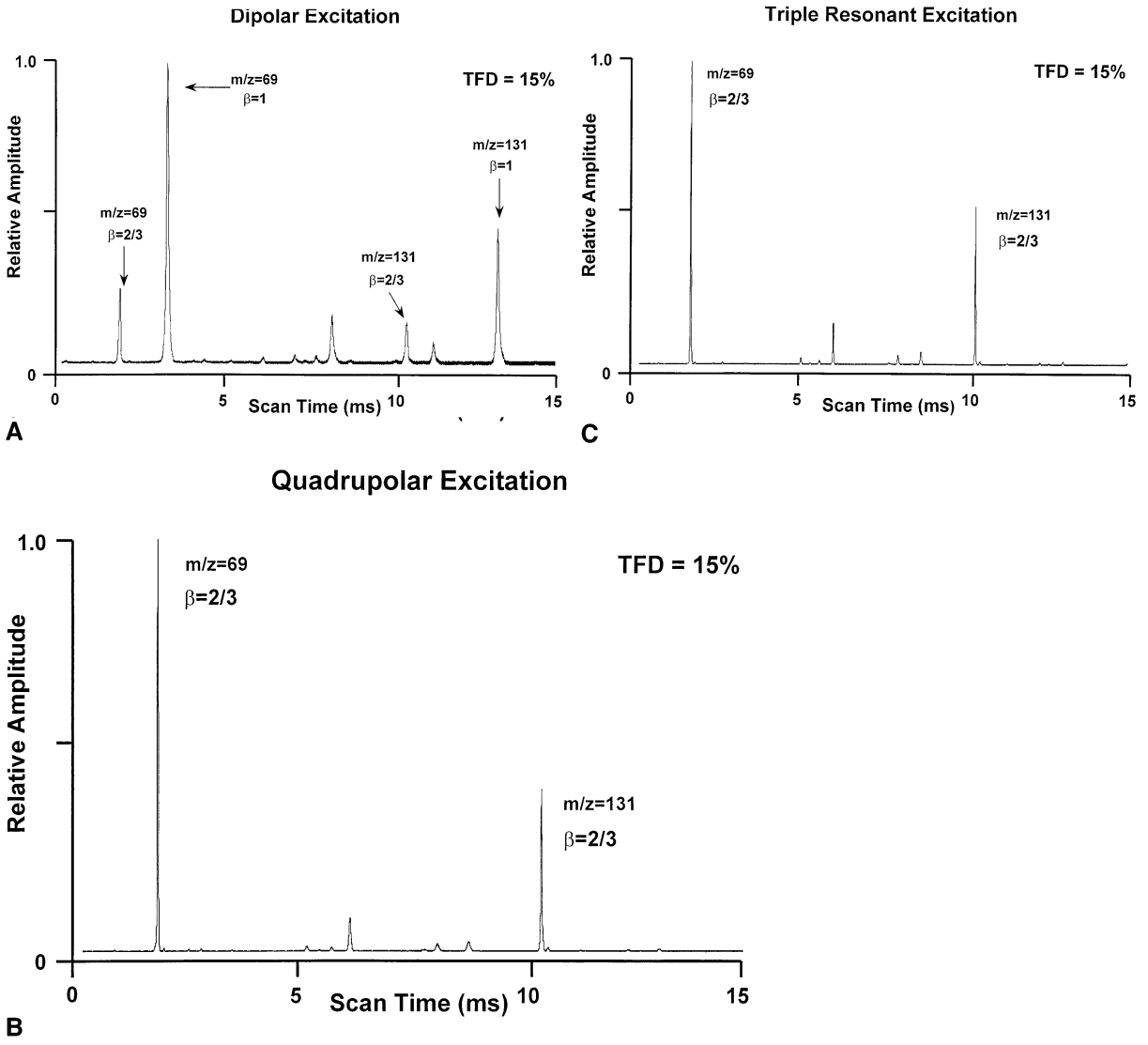

Fig. 6. Mass spectrum of FC-43 obtained with a 15% TFD. (a) Double resonance with the trapping field hexapole resonance and a supplementary dipole amplitude of 2 $V_{(p-p)}$ with a frequency of 700 kHz. (b) Double resonance with the trapping field hexapole resonance and a supplementary quadrupole amplitude of 10 $V_{(p-p)}$ with a frequency of 700 kHz. (c) Triple resonance with the combined supplementary dipole and quadupole fields used in (a) and (b).

shown in Fig. 7(a) and (b). Fig. 8(a) and (b) show the corresponding quantities for triple resonant excitation. The triple resonant ejection mode shows the axial position displaced 1 mm away from the center of the ion trap as a result of the 15% TFD. The ion axial motion was limited to small excursions, ±1 mm, and ion kinetic energy was less than 10 eV up to 0.025 ms prior to ejection. In contrast, dipolar resonant excitation cause larger ion excursions and kinetic energies above 10 eV up to 0.25 ms prior to ejection. Collisions that occurred during the period prior to ejection, when ion energy exceeded 10 eV, would cause dissociation of the ion. The resulting lower mass ions were usually at an operating point outside of the

Table 2
Frequencies of ion motion in kHz, for triple resonant ejection and the dipolar resonant mode

Frequencies	Triple resonant	Dipolar resonant
Ω	1050	1050
$\omega_{z,0}$	350	485
$\Omega - \omega_{z,0}$	700	565
$\Delta\omega$[a]	350	80
$2\omega_{z,0}$	700	970
Operating point	$\beta_z = 2/3$	$\beta_z = 0.92$

[a] Beats between the sideband and the fundamental frequency component $\Delta\omega = \Omega - 2\omega_{z,0}$.

stability boundary and would be ejected in the axial direction within a few microseconds [9,12]. Generally, the width at the base of a mass peak was 0.12 ms for the triple resonant ejection mode and 0.18 ms for the dipolar resonant ejection mode. Ions ejected in the triple resonant mode from collisional dissociation during the 0.025 ms prior to normal ejection had only a small effect on the peak symmetry. However, in the dipolar resonant mode, ions ejected during the 0.25 ms prior to normal ejection caused a shift in the mass centroid towards low mass.

Metastable ions, such as the molecular ion of *n*-butylbenzene (*m/z* 134) and the fragment ion $C_4F_9^+$ (*m/z* 219) from FC-43, had symmetrical peak shapes when they were mass analyzed by the triple resonant ejection mode. In contrast, an asymmetric peak shape was observed with the dipolar resonant ejection mode; the mass peak was skewed and tailing towards the low mass side of the mass spectrum because of dissociation prior to normal ejection.

Fig. 9 compares the mass spectrum of the molecular ion (*m/z* 156) of undecane for dipolar resonant and triple resonant ion ejection. The molecular ions of normal hydrocarbons are often weak or absent in mass spectra obtained from an ion trap. The helium damping gas pressure was calculated to be approximately 5–6 mTorr, and the trap temperature was 150 °C. The ion signal observed for the triple resonant ejection was considerably greater than that obtained with the dipolar resonant ejection mode. Only a factor of two

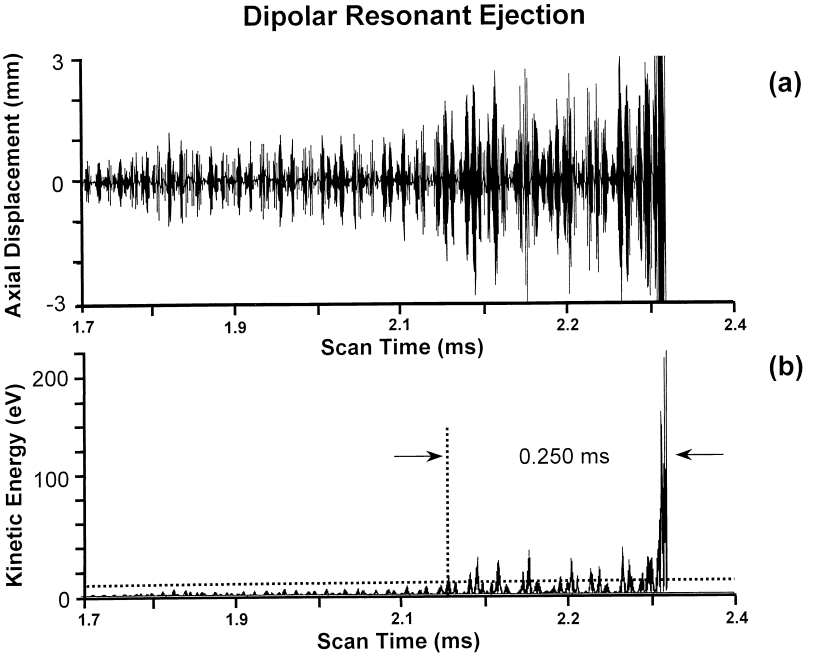

Fig. 7. (a) Simulation of the temporal variation of the axial position in mm for *m/z* 100 in a quadrupole tapping field. The ion is ejected at $\beta_z = 0.92$ with the dipolar resonant ejection mode. (b) Simulation of the ion kinetic energy in eV for the conditions of (a).

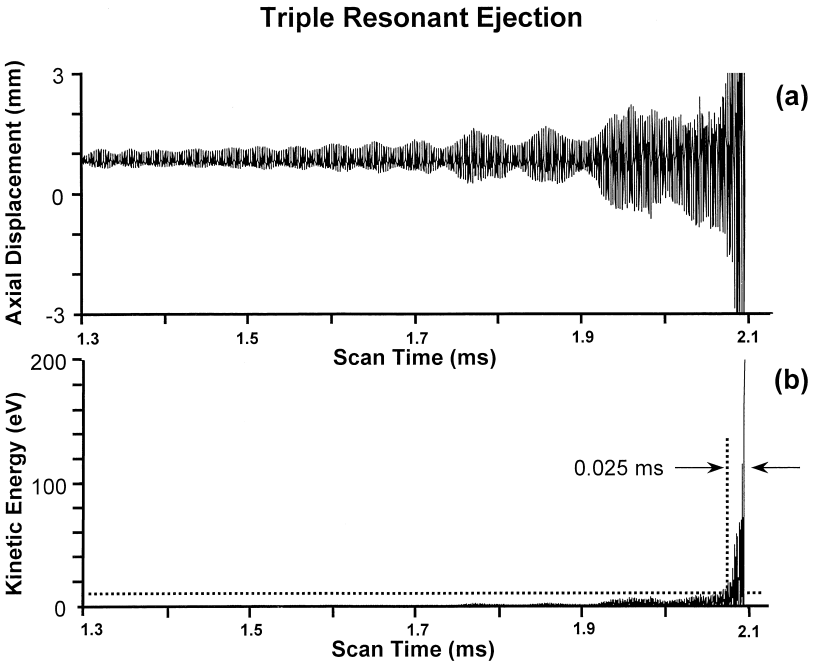

Fig. 8. (a) Simulation of the temporal variation of the axial position in mm for *m/z* 100 in an asymmetric trapping field. The ion is ejected at $\beta_z = 2/3$ with the triple resonant ejection mode. (b) Simulation of the ion kinetic energy in eV for the conditions of (a).

was expected because of the unidirectional ejection occurring with the triple resonant ejection mode. As discussed earlier, collisions that occur during the long ejection time required for dipolar resonant excitation can cause dissociation early in the excitation process, and will be immediately ejected at the instability boundary. This causes a reduction in the mass peak intensity and a shift of the mass centroid towards low mass. The ion ejection time for triple resonance is significantly shorter and few collisions will occur with ions of sufficient kinetic energy to cause dissociation. Therefore, the mass resolution was significantly improved for ions that had low thresholds for dissociation.

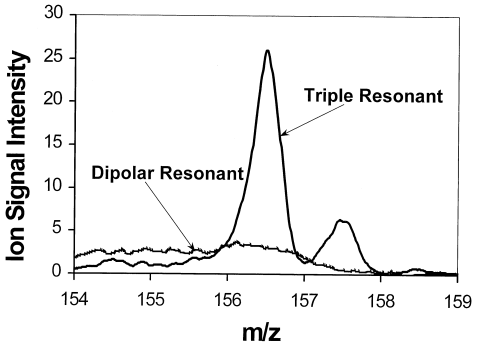

Fig. 9. Mass spectrum of the molecular ion of undecane (*m/z* 156) at a temperature of 150 °C and a helium pressure of 5.8 mTorr.

4. Conclusions

The data presented indicates that the addition of a "trapping field dipole" component to the normal "stretched" ion trap hyperbolic electrode geometry will generate both a dipole and a significant hexapole component in the trapping field. Further, the ions do not reside at the geometric center of the electrode assembly, but rather, they reside in a region between the electrodes displaced along the axis of the ion trap, away from the center. This asymmetric trapping field results in the ions being located at a position in which the hexapole field has a nonzero value. In addition,

because the ions do not reside at the geometrical center, any higher order multipole fields will have a nonzero value at this location. Therefore, if a supplementary quadrupole field is applied at a frequency such that the parametric oscillation corresponds to an operating point of $\beta_z = 2/3$, an ion located at this operating point will absorb power from both the hexapole resonance component of the trapping field and the quadrupole parametric resonance simultaneously. The addition of a weak dipole field corresponding to the first sideband resonance, at an operating point of $\beta_z = 2/3$ will also be in resonance simultaneously with the other two fields. This "triple" resonance results in a nonlinear power absorption that causes ion ejection.

In general, the triple resonance mass peak width is narrower and more symmetrical than that obtained by dipolar resonant ejection. The mass peak width and symmetry for quadrupolar double resonance ejection is similar to that of the triple resonance and occurs without the need for a supplementary dipole field. The removal of the supplementary dipole field causes a slight reduction in resolution, mostly at higher levels of space charge.

Acknowledgement

The authors gratefully acknowledge Brian Roussel for his technical assistance.

References

[1] R.E. March, R.J. Hughes, Quadrupole Storage Mass Spectrometry, Wiley, New York, 1991.
[2] J.E. Fulford, R.E. March, Int. J. Mass Spectrom. Ion Phys. 26 (1978) 155.
[3] J.E. Fulford, D.N. Hoa, R.J. Hughes, R.E. March, R.F. Bonner, G.J. Wong, J. Vac. Sci. Technol. 17 (1980) 829.
[4] K.B. Jefferts, Phys. Rev. Lett. 20 (1968) 39.
[5] E.S. Ensberg, K.B. Jefferts, Astrophys. J. 195 (1975) L89.
[6] G.C. Stafford, P.E. Kelley, D.R. Stephens, U.S. Patent No. 4,540,884; 1995.
[7] J.P. Syka, J.N. Louris, P.E. Kelley, G.C. Stafford, W.E. Reynolds, U.S. Patent No. 4,736,101; 1988.
[8] D.B. Langmuir, R.V. Lamgmuir, H. Shelton, R.F. Wuerker, U.S. Patent No. 3,065,640; 1962.
[9] R.L. Alfred, F.A. Londry, R.E. March, Int. J. Mass Spectrom. Ion Processes 125 (1993) 171.
[10] P.E. Kelley, U.S. Patent No. 5,381,007; 1995.
[11] J. Franzen, U.S. Patent No. 5,468,957; 1995.
[12] J. Franzen, R.H. Gabling, M. Shubert, Y. Wang, in R.E. March, J.F.J. Todd (Eds.), Practical Aspects of Ion Trap Mass Spectrometry, CRC, Boca Raton, FL, 1995, Vol. 1, Chap. 3.
[13] J.N. Louris, J. Schwartz, G.C. Stafford, J. Syka, D. Taylor, Proceedings of the 40th ASMS Conference on Mass Spectrometry and Allied Topics, Washington, DC, June 1992, p. 1003.
[14] J. Franzen, R.-H. Gabling, G.H. Grasberg, G. Weiss, U.S. Patent No. 4,975,577; 1990.
[15] J. Franzen, R.-H. Gabling, G.H. Grasberg, G. Weiss, U.S. Patent No. 5,028,777; 1991.
[16] J. Franzen, U.S. Patent No. 5,170,054; 1992.
[17] G. Wells, Proceedings of the 44th ASMS Conference on Mass Spectrometry and Allied Topics, Portland, OR, May 1996, p. 126.
[18] M. Wang, E.G. Marquette, U.S. Patent No. 5,291,017; 1994.
[19] G.J. Wells, M. Wang, E.G. Maquette, U.S. Patent No. 5,714,755; 1998.
[20] J.D. Williams, H.P. Reiser, R.E. Kaiser, R.G. Cooks, Int. J. Mass Spectrom. Ion Processes 108 (1991) 199.
[21] R.K. Julian, Ph.D. Thesis, Purdue University, 1993.
[22] F. Guidugli, P. Traldi, A.M. Franklin, M.L. Langford, J. Murell, J.F.J. Todd, Rapid Commun. Mass Spectrom. 6 (1992) 229.
[23] J. Franzen, Int. J. Mass Spectrom. Ion Processes 106 (1991) 63.
[24] J.D. Jackson, Classical Electrodynamics, Wiley, New York, 1967.
[25] E.C. Beaty, Phys. Rev. A 33 (1996) 3645.
[26] Y. Wang, J. Franzen, K.P. Wanczek, Int. J. Mass Spectrom. Ion Processes 124 (1993) 125.
[27] Y. Wang, Rapid Commun. Mass Spectrom. 7 (1993) 920.
[28] J. Franzen, Int. J. Mass Spectrom. Ion Processes 125 (1993) 165.
[29] J. Franzen, Int. J. Mass Spectrom. Ion Processes 130 (1994) 15.
[30] Y. Wang, J. Franzen, Int. J. Mass Spectrom. Ion Processes 132 (1994) 155.